Impact of Nanosecond Laser Annealing on the Formation of Titanium Silicides

Laura Esposito, Sebastien Kerdiles, Magali Gregoire, Dominique Mangelinck

Impact of Nanosecond Laser Annealing on the Formation of Titanium Silicides

Laura Esposito[1,2,3], Sébastien Kerdilès[1*], Magali Grégoire[2] and Dominique Mangelinck[3]

[1] Université Grenoble-Alpes, CEA-LETI, F-38000 Grenoble, France.
[2] STMicrolectronics, 850 rue Jean Monnet, F-38926 Crolles Cedex, France
[3] Institut Matériaux Microélectronique Nanosciences de Provence, IM2NP-CNRS, Aix-Marseille Université, Service 142 Faculté de St-Jérôme, F-13397 Marseille Cedex 20, France
* Presenting and contact author: sebastien.kerdiles@cea.fr

Abstract

In view of advanced image sensors, Ti silicides formation is explored by means of nanosecond laser annealing (NLA) combined to rapid thermal processing (RTP) to tentatively obtain ohmic contacts within a limited thermal budget. Leveraging sheet resistance and X-ray diffraction measurements, coupled to electron microscopy observations, the various phases obtained after NLA and after a subsequent RTP are identified and the involved mechanisms discussed.

1. Introduction

Thermal treatments in microelectronics kept evolving towards ever shorter processes to sustain the continuous device scaling. Anneals lasting a few seconds in RTP systems were first introduced to replace some of the long treatments in furnaces in the 1980's, mainly to enable the formation of shallow junctions and later to form electrical contacts [1]. After the 2000's, in order to further limit diffusion, millisecond anneals were also implemented leveraging flash lamps or continuous wave lasers [2]. Each time that an alternative thermal treatment has been necessary to improve device performance, lasers with sub-µs pulse duration have been considered, but such annealing technique has so far been rejected to the following generation successively by RTP and millisecond anneals for various reasons such as a poor laser stability, laser beam non-uniformity or strong pattern density issues [3-5].

New opportunities for NLA have more recently emerged and developments in this field experience a strong 'third' wave [6]. NLA, exposing the sample surface to a laser radiation during less than a µs, first enables to continue the trend towards shorter anneals at high temperatures. With the possibility to work in the melt or sub-melt regimes, and extremely high quenching rates, NLA enables record high dopant activation levels in both Si and Ge [7-8]. In addition to this 'evolutionary' opportunity detected since the 1980's, all the ingredients of a 'revolutionary' situation are now here to propel NLA as the unique solution for the coming device architectures. NLA, taking advantage of its short pulse duration, and advantageously combined with a short wavelength promoting the radiation absorption in the first nanometers, enables selective heating of the surface. This ability to reach extremely high temperatures at the irradiated surface while keeping the underlying structures at low temperatures, is unique and particularly suited for device fabrication with high thermal budget constraints. A first important example using NLA in mass production, is the processing of the wafer backside (dopant activation, ohmic contact formation) during the fabrication of Si or SiC insulated gate bipolar transistors (IGBT) while metallization is already present on frontside [9]. 3D sequential integration is another architecture for which NLA is currently investigated, particularly for dopant activation and/or gate annealing for the upper level(s) of active devices [10-12]. For advanced 3D architectures of CMOS image sensors, also exhibiting some thermal budget limitations, we investigated titanium silicide based contact formation using NLA [13].

The first Ti silicidation attempts leveraging NLA dealt with very thick Ti layers (from 140 to 400 nm) [14-15]. Formation of the high-resistivity phase C49-$TiSi_2$ was demonstrated with nevertheless a very limited understanding of the involved mechanisms. A few years later, Chen et al., starting from 35 nm Ti thick layers, succeeded in the formation of the low resistivity C54-$TiSi_2$ either directly after laser exposure [16] or after combination with a subsequent anneal at 600°C [17] using a Nd:YAG pulsed laser with a gaussian beam. They also obtained the C40-$TiSi_2$ phase without introduction of foreign metal at the Si/Ti interface. This phase was shown to promote the formation of the C54-$TiSi_2$ phase, bypassing the C49-$TiSi_2$ phase unavoidable in the classical approach using RTP only [18]. Nevertheless, the use of gaussian laser beams does not enable accurate control of the local laser energy density (ED). In particular, it is not clear whether the mechanisms responsible for the formation of the various phases occur in the solid or the liquid phase.

In view of advanced 3D CMOS image sensors, we explore in this work the Ti silicidation of much thinner Ti layers (10 nm) using a large and uniform pulsed laser beam (top hat profile) enabling an accurate laser ED control. The impact of the initial substrate nature is also investigated.

2. Experimental procedure

The surface of p-type (~1×10^{15} B/cm^3) 300 mm diameter Si(100) wafers was first cleaned using a diluted-HF solution and then a SC1 step. Under high vacuum, the surface oxide of the samples was removed using the SiCoNi™ process. Without air break, Ti and TiN layers were then deposited with 10 nm target thickness for both layers. The samples were subsequently annealed using ultraviolet NLA (UV-NLA) only or coupling UV-NLA and RTA. For laser

exposure in N_2, we used the SCREEN LT-3100 platform, based on a XeCl excimer laser (λ=308 nm, pulse duration = 160 ns). The laser beam was a 15×15 mm² top hat profile with a homogeneity better than 2.5% within each field. The laser ED was accurately explored from 0.3 to 1.0 J/cm² and the number of laser shots at the same location was set to 1, 3, 10, 30 or 100. RTA was performed in N_2 at temperatures ranging from 550 to 950°C, during 30 seconds, using a Levitor4300 system from Levitech.

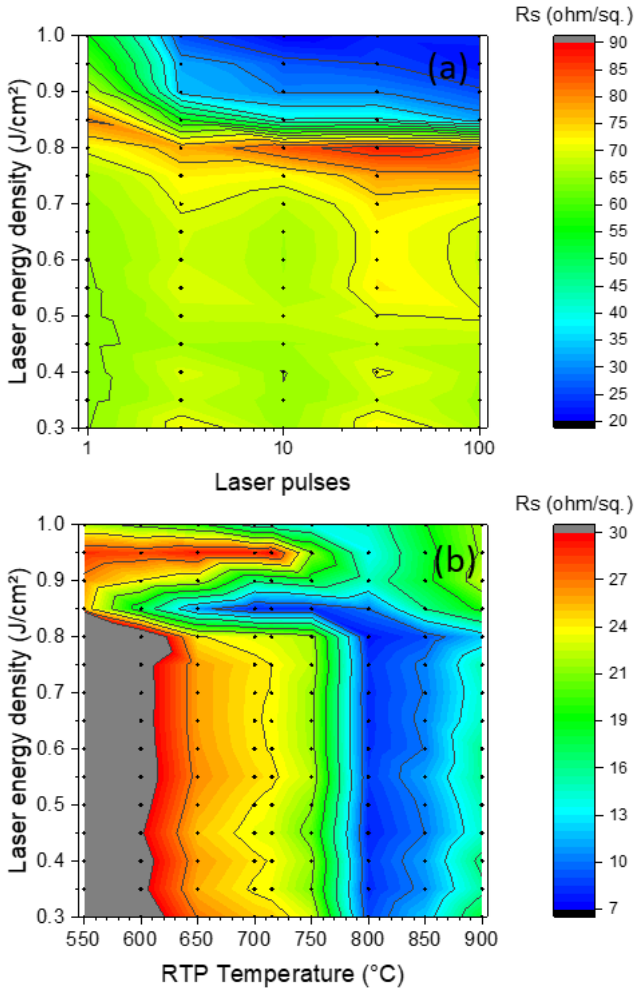

Fig. 1 Sheet resistance evolution (a) after laser annealing as a function of ED and the number of pulses, (b) after laser and a subsequent RTP as a function of ED and the RTP temperature.

The sheet resistance, Rs, of the samples was measured by the 4 point-probe method using a NAPSON tool. X-ray diffraction (XRD) measurements were conducted to extract the various crystalline phases present in the samples. Structural information was also extracted from high resolution transmission electron microscopy (HRTEM) cross-sections. The surface of the annealed samples was also observed by scanning electron microscopy (SEM). Numerical simulations were finally performed using LIAB software, to estimate the temperature as a function of time and depth for each laser ED value explored experimentally. Details on the simulation tool can be found in [19] and references therein.

Most of the results presented hereafter deal with the lightly doped p-type Si substrates. Nevertheless, to investigate the effect of the initial substrate nature and doping level, the same approach has also been applied to phosphorus doped monocrystalline Si substrates, hereafter labelled n+ doped c-Si, and to phosphorus doped polycrystalline layers deposited on Si substrates, hereafter named n+ doped poly-Si. Details on the preparation of these doped substrates can be found in [20].

3. Results and discussion

The sheet resistance of the samples exposed to UV-NLA is shown in Fig.1(a) as a function of the laser ED and the number of pulses. Below 0.750 J/cm², Rs remains at the level measured right after Ti/TiN deposition, around 70 Ω/sq. In the 0.750-0.825 J/cm² range, Rs increases, exceeding 85 Ω/sq. for 3 pulses and beyond (red/orange region in the Rs map). Except for 1 laser pulse, from 0.825 to 1.000 J/cm², Rs decreases to ~35 Ω/sq at 0.875 J/cm² then down to 20-25 Ω/sq. in the 0.900-1.000 J/cm² range (blue region in the Rs map).

Figure 1(b) displays the evolution of Rs for the samples submitted to three UV-NLA pulses at various ED values and a subsequent RTP at temperatures ranging from 550 to 950°C. In the 0.300-0.800 J/cm² range, Rs only depends on the RTP temperature, with a minimum at around 10 Ω/sq. at 800-850°C (vertical part of the blue region in the Rs map). It corresponds to the classical RTP process condition leading to the technologically interesting C54-$TiSi_2$ phase. Surprisingly, for ED values around 0.850 J/cm² and RTP temperature from 650°C to 800°C, Rs exhibits a minimum still around 10 Ω/sq. or slightly below (horizontal blue valley in the Rs map), corresponding to the formation of a low resistive silicide phase at moderate thermal budget. This sharp minimum measured after laser and RTP is obtained for laser conditions leading to the abrupt Rs decrease after laser. In order to understand such Rs evolution after laser or after laser combined to RTP, further characterizations were conducted, in particular to elucidate the various phases obtained.

Figure 2(a) and 2(b) respectively show the normalized XRD profiles of the samples exposed to three laser pulses at various ED values, and those submitted to the same laser treatment and a subsequent RTP at 650°C during 30 seconds. After laser only, up to 0.75 J/cm², XRD profiles remain similar to those corresponding to the as-deposited samples (not shown), with three peaks identified as TiN, $TiNO_x$ (or TiO_2) and Ti. When increasing ED from 0.75 to 0.85 J/cm², Ti peak vanishes indicating the progressive Ti consumption. No new peak being detected in parallel, this Ti consumption is likely resulting in the formation of an amorphous silicide phase (a-$Ti_{1-X}Si_X$), responsible for the concomitant Rs increase. Above 0.90 J/cm², except the constant TiN peak, XRD profiles exhibit a peak at 40.5°, characteristic of the C40-$TiSi_2$ phase. The minimum Rs valley after laser

annealing, i.e. the blue region in Fig.1(a), is thus corresponding to the full conversion of the deposited Ti into C40-$TiSi_2$ by UV-NLA with at least 3 pulses at 0.90 J/cm² and beyond.

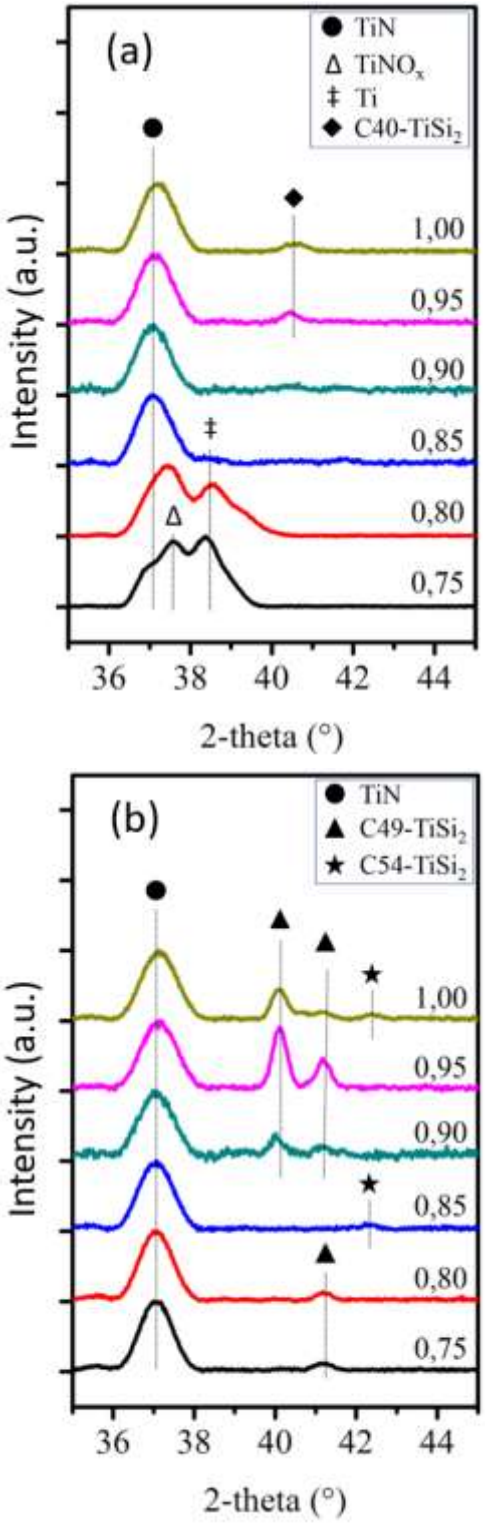

Fig. 2 XRD profiles of the TiN/Ti/Si samples (a) annealed with 3 laser pulses at the indicated ED values (J/cm²), (b) submitted to the same laser treatment and a subsequent RTP at 650°C.

After 3 laser pulses and RTP at 650°C, XRD profiles all exhibit a TiN peak used for normalization. In addition to TiN, for 0.75 and 0.80 J/cm², the high resistivity C49-$TiSi_2$ phase is evidenced. After 3 laser pulses at 0.85 J/cm² coupled to a RTP at 650°C, only the C54-$TiSi_2$ phase is detected, which is consistent with the minimum Rs value obtained for this specific condition, and for a higher number of pulses at the same ED. This particular process condition demonstrates that it is possible to reduce the C54-$TiSi_2$ formation temperature down to 650°C using an appropriate pulsed laser pre-treatment, not only starting from thick Ti layers as reported by Chen et al.[18], but also with 10 nm thin Ti initial layers. For higher ED values, i.e. 0.90 J/cm² and beyond, C49-$TiSi_2$ is again detected, eventually mixed with the C54-$TiSi_2$ phase at 1.00 J/cm². Despite the formation of the C40-$TiSi_2$ phase, supposed to promote the C54-$TiSi_2$ phase formation [18,21], for multiple laser process conditions, a subsequent RTP does not systematically convert it into C54-$TiSi_2$.

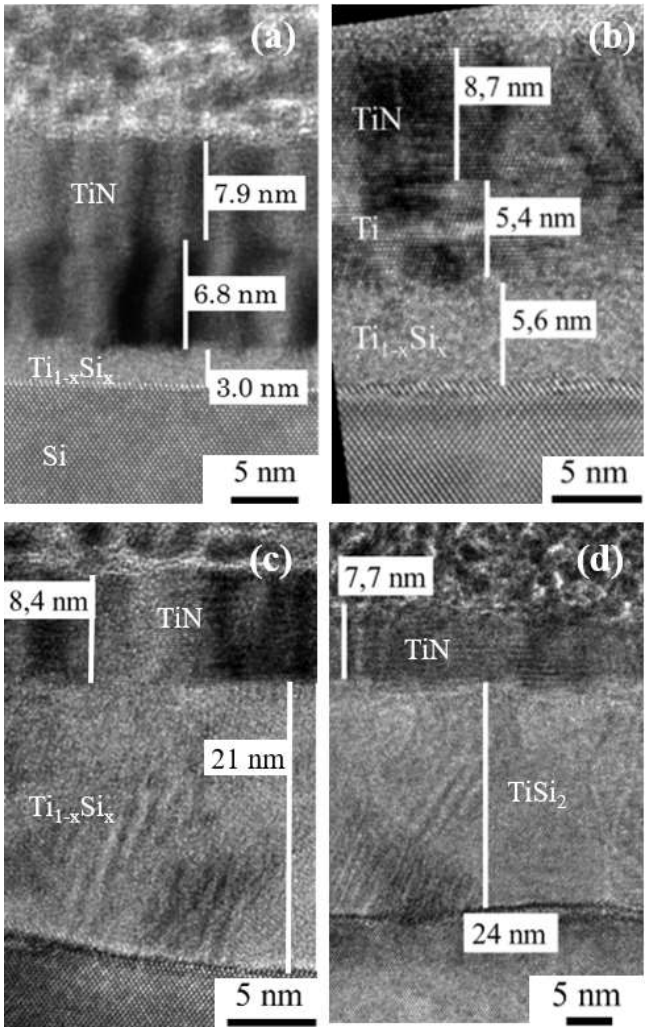

Fig. 3 HRTEM cross-section observation of the TiN/Ti/Si samples (a) after deposition, and after annealing using 3 laser pulses at (b) 0.80 J/cm², (c) 0.85 J/cm² and (d) 1.00 J/cm².

To elucidate the exact configuration leading to the desired phase in our case, HRTEM observations were performed on samples after deposition and after laser treatment using 3 pulses, as displayed in Fig.3. After Ti and TiN deposition, a 3 nm thin amorphous intermixing layer is evidenced at the Si/Ti interface and a 6.8 nm thick Ti layer on top (Fig.3(a)). After three pulses at 0.80 J/cm², we observe, from top to bottom, a 8.7 nm TiN layer, a 5.4 nm Ti film, a 5.6 nm thin a-$Ti_{1-X}Si_X$ layer and the Si substrate. Fig.3(b) confirms the partial Ti consumption evidenced by XRD and the formation of an amorphous silicide in this case. For three laser pulses at 0.85 J/cm² (Fig.3(c), Ti is fully consumed and the silicide exhibit a non-uniform thickness with variations from 17 to 21 nm. For this specific laser conditions leading to the C54-$TiSi_2$ phase after a subsequent RTP at 650°C, the obtained silicide is at least partially crystalline, with some nanocrystals likely embedded in an amorphous matrix. We believe that these observed nanocrystals correspond to the early stages of the C40-$TiSi_2$ phase formation that is better evidenced from 0.90 J/cm² by XRD. Finally, at 1.00 J/cm² (3 pulses), the obtained silicide is clearly crystalline (C40-$TiSi_2$ phase according to XRD profiles) with a thickness around 24 nm.

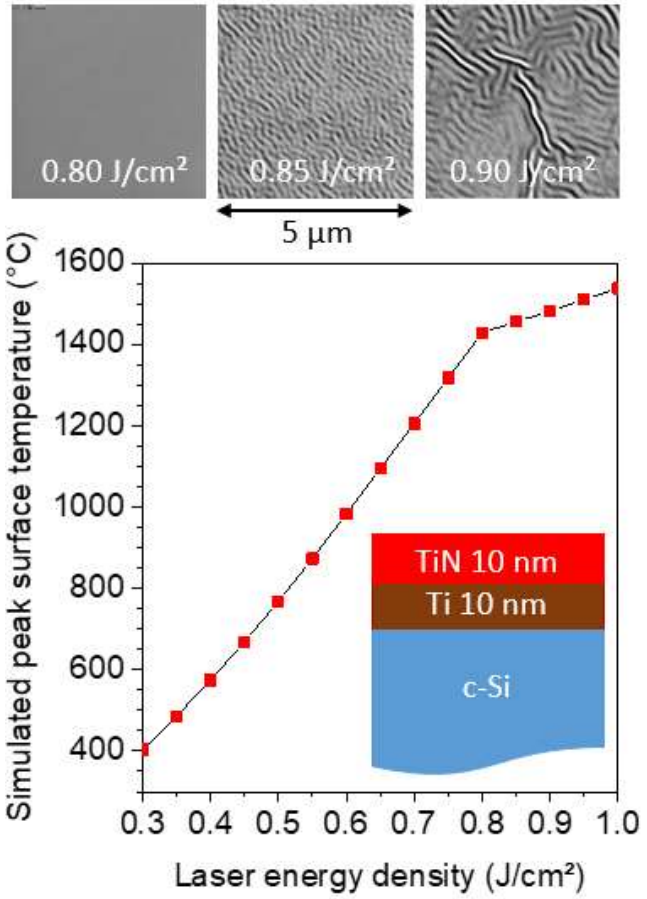

Fig. 4 Simulated maximum surface temperature during laser exposure as a function of the ED irradiating the simplified stack shown in inset. Top view SEM observations of the sample surface after three laser pulses are shown for three indicated ED settings.

Unlike previous studies on Ti silicidation using NLA with a gaussian laser beam [16-18,21], we can control more accurately the effectively delivered ED thanks to a uniform top hat intensity profile, without assuming an average ED over a gaussian profile. It's particularly important to identify from which ED value the mechanisms involved in this silicidation process switch from the solid phase to the liquid phase.

To do so, we conducted 1D numerical simulations gathered in Fig.4. The maximum surface temperature is calculated as a function of the ED irradiating the simplified stack, shown in Fig.4., in which no initial amorphous silicide is taken into account. When increasing the laser ED from 0.30 to 0.80 J/cm², the maximum surface temperature increases quasi-linearly and reaches the Si melting point around 0.80 J/cm². Above this critical value, the surface temperature still increases but more moderately due to the higher reflectivity of the liquid phase on one hand, and the latent heat of fusion effect, on the other hand. Taking into account the very slight temperature gradient from the surface to the substrate, the melt of the upper nanometers of silicon is predicted by our simulations slightly above 0.80 J/cm². The top-view SEM surface observations shown in the upper part of Fig.4 lead to a perfect match between the simulations and the experimental data. Indeed, the surface remains flat up to 0.80 J/cm² while it exhibits some wrinkles with an increasing amplitude from 0.85 J/cm² and above. These wrinkles would result from the stress relaxation of an elastic capping layer remaining solid during the laser pulse while a sufficiently thick liquid layer is transiently generated between this capping and the rigid substrate [22,23]. In our case, during the laser pulse (for ED in the 0.80-1.00 J/cm² range), at least the compressive TiN film remains solid and tends to relax, leading to wrinkles, as soon a thin liquid layer appears during the laser pulse. This liquid layer is very likely made of silicon but it could originate as well from the melt of the a-$Ti_{1-X}Si_X$ phase whose melting point is expected close to that of silicon or even below. The wrinkles observed by SEM at the surface also correspond to the thickness variations of the silicide layer evidenced by HRTEM in Fig. 3(c) and (d). Thus, both SEM observations and numerical simulations indicate that phenomena discussed for samples with a p-type substrate and for ED values between 0.30 and 0.80 J/cm² correspond to mechanisms in the solid phase. In particular, Ti consumption and the concomitant formation of the amorphous a-$Ti_{1-X}Si_X$ phase occur in the solid phase. In contrast, as long as ED exceeds 0.80 J/cm², we can expect some reactions in the liquid phase. The formation of the C40-$TiSi_2$ phase is likely only happening in the liquid phase, as suggested by D'Anna et al. for several silicides obtained by pulsed laser annealing [14,24]. The very specific laser condition (3 pulses at 0.85 J/cm²) enabling, after a subsequent RTP at 650°C, the formation of the C54-$TiSi_2$ phase is expected to correspond to the very beginning of the liquid phase appearance.

In view of advanced image sensors fabrication, Ti silicidation is targeted simultaneously on various regions,

some of them being monocrystalline or polycrystalline silicon, either doped or undoped. The impact of such initial surface to be contacted has thus to be investigated. Figure 5 provides a summary of the various phases detected after laser treatment only and after laser annealing followed by a RTP at 650°C for TiN/Ti/Si samples based on p-type lightly doped c-Si (labelled 'undoped c-Si'), n+ c-Si and n+ poly-Si. The phases detected either by XRD measurements and/or HR-TEM observations are plotted as a function of the applied ED in the case of three laser pulses, except TiN that is systematically present but not mentioned. The phases reported for the undoped c-Si case correspond to the results discussed so far (plain bars in Fig.5).

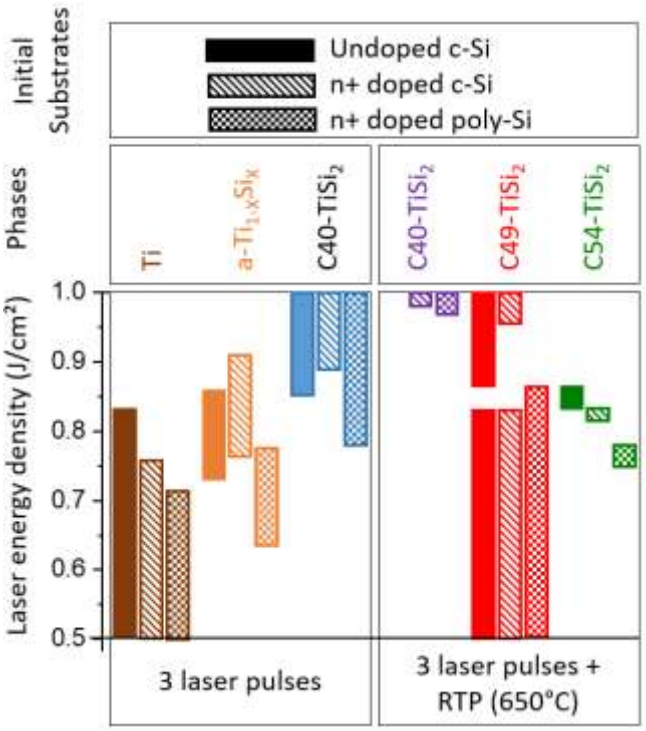

Fig. 5 Detected phases in TiN/Ti/Si samples submitted to three laser pulses as a function of the laser ED, after UV-NLA and after UV-NLA combined to RTP at 650°C. The samples based on a lightly p-type doped monocrystalline Si substrate ('Undoped c-Si') are compared to equivalent samples based on n+ doped monocrystalline Si substrates or polycrystalline layers.

Whatever the nature of the substrate, the same three phases are detected after laser annealing, namely Ti, a-$Ti_{1-x}Si_x$ and C40-$TiSi_2$, with some ED shifts. Ti consumption occurs at lower ED values in the case of doped monocrystalline substrates, and even lower for doped poly-Si. For this latter kind of substrate, the amorphous silicide phase and C40-$TiSi_2$ are formed at ED values about 15% lower than for monocrystalline substrates. After laser treatment coupled to RTP at 650°C, C49-$TiSi_2$ phase is present for most of the tested laser conditions whatever the initial substrate. For doped substrates, C54-$TiSi_2$ phase has been obtained as well but still within a narrow range of ED values, systematically mixed with the C49-$TiSi_2$ phase, and not for the same ED values as for the undoped substrate. Thus, none of the explored process conditions enables the formation of the sole C54-$TiSi_2$ phase simultaneously for the three tested substrates. The ED shift due to doping is found relatively limited but the effect of the polycrystalline nature of the Si reacting with Ti is more pronounced. The grain size may affect both the laser radiation absorption and the melting point of the Si layer. Finally, C40-$TiSi_2$ is detected for n+ doped substrates around 1.00 J/cm², which is not the case for the undoped substrate but it might occur in this case for ED values slightly higher, i.e. out of the range investigated in this work.

3. Conclusions

Ti silicide formation using UV-NLA eventually combined with RTP has been explored, starting from thin Ti layers and leveraging a top-hat uniform laser beam to accurately control the applied laser energy density. The samples have been submitted to sheet resistance and XRD measurements, SEM and HRTEM observations to study their electrical behavior and the obtained phases. After the sole use of UV-NLA, whatever the ED setting and the number of laser pulses, neither the C49-$TiSi_2$ nor the C54-$TiSi_2$ phase have been directly formed. A subsequent RTP is required. In the case of p-type Si monocrystalline substrate, for ED up to 0.80 J/cm², UV-NLA leads to the growth by solid phase reaction of an amorphous silicide, resulting from the consumption of the deposited Ti layer and responsible for a sheet resistance increase. From 0.90 J/cm² and above, UV-NLA enables the formation of the C40-$TiSi_2$ phase by reaction in the liquid state. In between, i.e. around 0.85 J/cm² (for at least 3 pulses), an intermediate state in generated with silicide nanocrystals, likely C40-$TiSi_2$ phase, embedded in an amorphous silicide matrix. Such sample subsequently annealed by RTP at 650°C results in the formation of the sole low resistivity C54-$TiSi_2$ phase. For lower or higher ED settings, the C49-$TiSi_2$ phase is obtained after RTP. The same phases can be obtained using the same process sequence but starting from n+ doped monocrystalline or polycrystalline silicon substrates instead. Nevertheless, n+ doping and mainly the polycrystalline nature of the Si substrate induces a shift of the different phases consumption and formation or transformation, towards lower ED values. C54-$TiSi_2$ phase has been obtained in each case but none of the tested process enables the formation of this sole phase simultaneously on the three different substrates. Additional work is needed to identify a common process window.

Acknowledgements

SCREEN Company and its French subsidiary LASSE are gratefully acknowledged for their support in operating and maintaining the LT-3100 nanosecond laser annealing platform.

References

[1] A. Cullis, Rep. Prog. Phys. 48, 1155 (1985)

[2] W. Skorupa and H. Schmidt, 'Sub-second annealing of advanced materials', Springer (2014)

[3] Y. Jin, Y. Zhao and Y. Jiang, J. Laser Appl., 28, 022601 (2016)

[4] P. Morin, F. Cacho, R. Beneyton, B. Dumont, A. Colin, H. Bono, A. Villaret, E. Josse and R. Bianchini, Solid-State Electr. 54, 897 (2010)

[5] R. Delmdahl and R. Pätzel, J. Phys. D Appl. Phys., 47, 034004 (2014)

[6] K. Huet, F. Mazzamuto, T. Tabata, I. Toqué-Tressonne and T. Mori, Mat. Sci. Semic. Proc. 62, 92 (2017)

[7] S. Solmi, E. Landi, F. Baruffaldi, J. Appl. Phys. 68(7), 3250 (1990)

[8] G. Masetti, M. Severi, S. Solmi, IEEE Trans. Electr. Dev. 30(7), 764 (1983)

[9] R. Rupp, R. Kern and R. Gerlach, Proc. 25th Int. Symp. Power Semicond. Devices and ICs, 6694396, pp.51 (2013)

[10] C. Fenouillet-Béranger et al., Techn. Digest IEDM conference, 7047121, pp.27 (2015)

[11] L. Brunet et al., Techn. Digest IEDM conference, 8614653, pp.7.2.1 (2019)

[12] A. Vandooren et al., VLSI Conference Techn. Digest, 9265026 (2020)

[13] L. Esposito, S. Kerdilès, M. Grégoire, P. Benigni, K. Dabertrand, J.-G. Mattei, and D. Mangelinck, J. Appl. Phys. 128, 085305 (2020)

[14] E. D'Anna, G. Leggieri, A. Luches, M. Martino, A. Perrone, Appl. Surf. Sci. 54, 353 (1992)

[15] V. Craciun, D. Craciun, N. Chitica, I. Mihailescu, L. Nistor, A. Popa, V. Teodorescu, I. Ursu, A. Kuzmichev, V. Konov, A. Prokhorov, G. Leggieri, A. Luches, M. Martoni, J. Phys. D Appl. Phys. 25, 1500 (1992)

[16] S. Chen, Y. Chen, Z. Chen, L. Chan and A. See, Appl. Phys. Lett. 75, 1727 (1999)

[17] S. Chen, Z. Chen, K. Li, A. See and L. Chan, Appl. Phys. Lett. 77, 4395 (2000)

[18] S. Chen, Z. Chen, A. See and L. Chan, J. Electrochem. Soc. 148 (12), G734 (2001)

[19] K. Huet, J. Aubin, P.-E. Raynal, B. Curvers, A. Verstraete, B. Lespinasse, F. Mazzamuto, A. Sciuto, S.F. Lombardo, A. La Magna, P. Acosta Alba, L. Dagault, C. Licitra, J.-M. Hartmann and S. Kerdilès, Appl. Surf. Sci., 505 (2020) 144470

[20] L. Esposito, S. Kerdilès, M. Grégoire, A. Newman, K. Dabertrand, B. Saidi, S. Joblot and D. Mangelinck, to be published in Micro. Eng. (2021)

[21] S. Chen, Z. Chen, S. Xu, C. Ong, A. See and L. Chan, J. Electrochem. Soc. 149 (11), G609 (2002)

[22] L. Benaissa and J.-S. Moulet, US patent 10357917 B2 (2019)

[23] R. Huang, J. Mech. Phys. Solids 53, 63 (2005)

[24] E. D'Anna, G. Leggieri and A. Luches, Thin Solid Films 218, 95 (1992)